# Hund's rule in superatoms with transition metal impurities

Victor M. Medel[a], Jose Ulises Reveles[a], Shiv N. Khanna[a,1], Vikas Chauhan[b], Prasenjit Sen[b], and A. Welford Castleman[c]

[a]Department of Physics, Virginia Commonwealth University, Richmond, VA 23284; [b]Harish-Chandra Research Institute, Chhatnag Road Jhunsi, Allahabad 211019, India; and [c]Departments of Chemistry and Physics, Pennsylvania State University, University Park, PA 16802

Edited by R. Stephen Berry, University of Chicago, Chicago, IL, and approved April 29, 2011 (received for review January 4, 2011)

**The quantum states in metal clusters bunch into supershells with associated orbitals having shapes resembling those in atoms, giving rise to the concept that selected clusters could mimic the characteristics of atoms and be classified as superatoms. Unlike atoms, the superatom orbitals span over multiple atoms and the filling of orbitals does not usually exhibit Hund's rule seen in atoms. Here, we demonstrate the possibility of enhancing exchange splitting in superatom shells via a composite cluster of a central transition metal and surrounding nearly free electron metal atoms. The transition metal d states hybridize with superatom D states and result in enhanced splitting between the majority and minority sets where the moment and the splitting can be controlled by the nature of the central atom. We demonstrate these findings through studies on $TMMg_n$ clusters where TM is a 3d atom. The clusters exhibit Hund's filling, opening the pathway to superatoms with magnetic shells.**

magnetic superatoms | jellium model | superatomic shells

The quantum confinement of electrons in small compact symmetric metal clusters results in electronic shell sequence 1S, 1P, 1D, …, much in the same way as in atoms. This analogy, originally introduced through the electronic states in a "jellium sphere" where the electron gas is confined to a uniform positive background of the size of the cluster, extends beyond this oversimplified model (1–9). Numerous first principles electronic structure studies on metal clusters have demonstrated the close grouping of electronic states into shells and have further shown that the shapes of the cluster electronic orbitals resemble those in atoms. Experiments on the reactivity of clusters have provided evidence that clusters and atoms of similar valence shells exhibit analogous chemical patterns. For example, although bulk aluminum is readily oxidized by oxygen, an $Al_{13}^-$ cluster with filled $1S^2$, $1P^6$, $1D^{10}$, $2S^2$, $1F^{14}$, and $2P^6$ shells exhibits strong resistance to etching by oxygen typical of inert atoms (5, 10). Further $Al_{13}$ has a large electron affinity of 3.4 eV close to that of a Cl atom (9). These analogies have prompted the concept that selected stable clusters could mimic the electronic behavior of elemental atoms and be classified as superatoms forming a third dimension of the periodic table (10–21). Because the properties of clusters change with size and composition, the superatoms offer the prospect of serving as the building blocks of nanomaterials with tunable characteristics (16, 18).

The electronic orbitals in superatoms, although resembling those in real atoms in shape, do spread over multiple atoms. This affects the way in which the electrons fill the shells because of two competing effects. Hund's rule favors high spin states in open shell systems stabilized by exchange coupling, and indeed higher spin multiplicities have been seen in some clusters (22) and even quantum dots spanning several nanometers (23). However, unlike the case of atoms, small clusters can undergo structural distortion that stabilizes the clusters through Jahn–Teller effect (24). Generally, the energy gain through Jahn–Teller distortion dominates, and unless the structural distortions are minimized by constraining the shape of the cluster, the filling of the electronic orbitals does not follow Hund's rule of maximizing the spin and result in superatoms with pairs of electrons favoring nonmagnetic character.

Recently we extended the concept of superatoms to magnetic species in which atomic d-state electrons localized on a transition metal site provide the spin magnetic moment, whereas delocalized electrons from the s-valence states of alkali atoms and of the transition metal atom occupy the diffuse superatomic S, P states (18–20). This results in species stabilized by filled superatom shells while localized atomic d states breed the magnetic moments.

An important issue is whether magnetic superatoms with intrinsic spin moments originating in superatom shells could be stabilized. Here we demonstrate that exchange splitting in these shells can be enhanced via composite clusters with a transition metal atom at the center. Through first principles electronic structure studies that focus on $FeMg_n$ ($n \leq 12$) and $TMMg_8$ (TM = 3d transition metal atoms) clusters, we show that the exchange split atomic d states of TM hybridize with D orbitals of the superatom leading to 1D and 2D superatom orbitals that have large exchange splitting and fill to maximize the total spin as in Hund's first rule in atoms. Unlike the case of atoms, partially filled shells also exhibit a previously undescribed feature. The clusters can open large gaps via a crystal field like splitting of the shells due to the arrangement of ionic cores much in the same way as crystal field splitting of atomic d states through the electric fields of surrounding ions in solids. One can thus open large gaps in partially filled subshells that can enhance chemical stability. We demonstrate these intriguing effects first through investigations on $FeMg_n$ clusters to show that an $FeMg_8$ is a highly stable magnetic superatom with a closed core of $1S^2$, $1P^6$, $1D^{10}$, and $2S^2$ superatom shells and a crystal field split $2D^4$ valence state resulting in a magnetic moment of 4.0 $\mu_B$ and a large gap of 0.64 eV between the highest occupied and lowest unoccupied molecular orbitals (HOMO-LUMO gap). Through subsequent studies on $TMMg_8$ atoms, we then demonstrate gradual filling of majority D manifold as the TM atom is changed and how the moment and the splitting can be controlled via the choice of TM atom.

## Results and Discussion

The valence configuration of a Mg atom is $3s^2$ and a $Mg_2$ is a weakly bound van der Waal molecule. However, bulk magnesium is a metal and earlier studies have shown that, in small clusters, the metallic character rapidly builds as multiple Mg atoms are brought together. The transition to metallic character occurs via the mixing of the *p* states, which are unfilled in the atom, with the *s* states. Previous studies on pure $Mg_n$ clusters indicate that there is already appreciable *p* character in the valence distribution for clusters containing as few as five atoms marking the

Author contributions: S.N.K. designed research; V.M.M., J.U.R., V.C., and P.S. performed research; A.W.C. analyzed data; and S.N.K. and J.U.R. wrote the paper.

The authors declare no conflict of interest.

This article is a PNAS Direct Submission.

[1]To whom correspondence should be addressed. E-mail: snkhanna@vcu.edu.

This article contains supporting information online at www.pnas.org/lookup/suppl/doi:10.1073/pnas.1100129108/-/DCSupplemental.

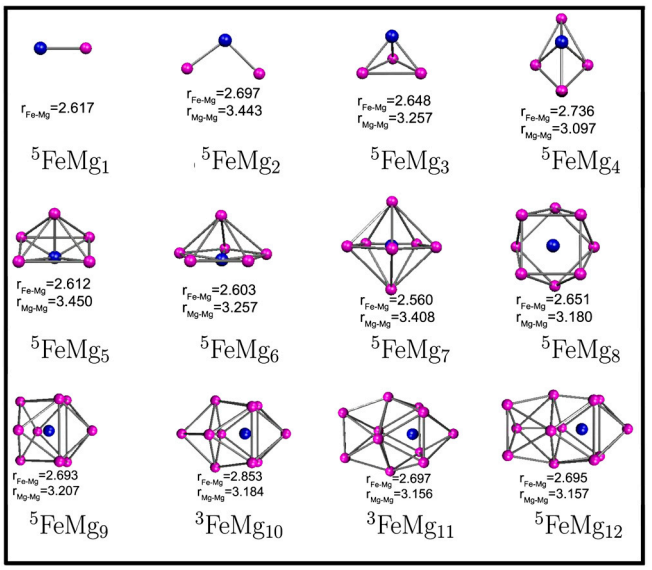


**Fig. 1.** Ground-state geometries of $FeMg_n$ ($n$ = 1–12) clusters. The superscripts indicate spin multiplicity. Blue and pink circles represent, respectively, Fe and Mg atoms.

presence of metallic character (25). The valence configuration of an Fe atom is $3d^64s^2$ with a spin multiplicity of 5. Theoretical studies indicate that the up and down spin manifolds in the Fe atom are separated by 0.8 eV (26). We wanted to examine how the valence character and the spin multiplicity evolve as Mg atoms are successively added to a Fe atom.

Fig. 1 shows the evolution of the ground-state geometry of $FeMg_n$ clusters. The ground-state structures are all compact with a Mg-Mg bond length ranging from 3.09 to 3.45 Å and Fe-Mg bond length varying between 2.56 and 2.85 Å. $FeMg_7$, with Mg atoms forming a pentagonal bipyramid, is the smallest cluster to contain an interior Fe atom. Studies where a Fe atom was forced to occupy an exterior site resulted in states that were 0.27 eV higher in energy. The structure of $FeMg_8$ is quite intriguing. The Mg sites form a square antiprism with an interior Fe atom. $FeMg_9$ has a Mg atom added to the square face of the biprism $FeMg_8$. Finally $FeMg_{12}$ is a hexagonal cage of Mg sites with an interior Fe atom.

Because the $Mg_n$ clusters become metallic with increasing size, we wanted to probe if $FeMg_n$ clusters would exhibit any electronic shell effects. The quantity of interest is the change in binding energy as successive Mg atoms are added, and the progression of the spin magnetic moment. The change in binding was monitored through incremental binding energy, $\Delta E_n$, calculated using the equation

$$\Delta E_n = E(Mg) + E(FeMg_{n-1}) - E(FeMg_n). \quad [1]$$

Here E(Mg), $E(FeMg_{n-1})$, and $E(FeMg_n)$ are the total energies of a Mg atom, $FeMg_{n-1}$ cluster, and $FeMg_n$ cluster, respectively. $\Delta E_n$ represents the gain in energy as an Mg atom is added to the preceding size $FeMg_{n-1}$. Fig. 2*A* shows $\Delta E_n$ as a function of $n$. There is a distinct maximum at $FeMg_8$. More importantly, there is a sharp drop in $\Delta E$ immediately following $FeMg_8$. The maxima and a sharp drop are both hallmarks of the enhanced stability and the associated magic character, seen previously in numerous metal clusters including pure $Na_n$ clusters (1). We also looked at the change in the HOMO-LUMO gap, again a signature of the enhanced stability in pure $Na_n$ clusters. Fig. 2*B* shows these variations and $FeMg_8$ also has a large HOMO-LUMO gap reinforcing the magic assignment. Although all these point to the magic character, it does raise an important issue. As the electronic structure of a Fe atom is $3d^64s^2$, the addition of 8 Mg atoms creates a valence pool of 24 electrons and, ordinarily, it does not correspond to the electron count for a shell filling within a confined electron gas. The origin of magic character of $FeMg_8$, therefore, has to be found elsewhere.

A single Fe atom has a spin multiplicity of 5 with four unpaired d electrons. We therefore examined the variation of the spin magnetic moment as successive Mg atoms were added. Fig. 2*C* shows the variation of the spin magnetic moment. $FeMg_8$ has a spin magnetic moment of 4.0 $\mu_B$. In fact, the spin magnetic moment of the free Fe atom is maintained up until 9 Mg atoms and then it drops. To examine the resilience of the magnetic state, we

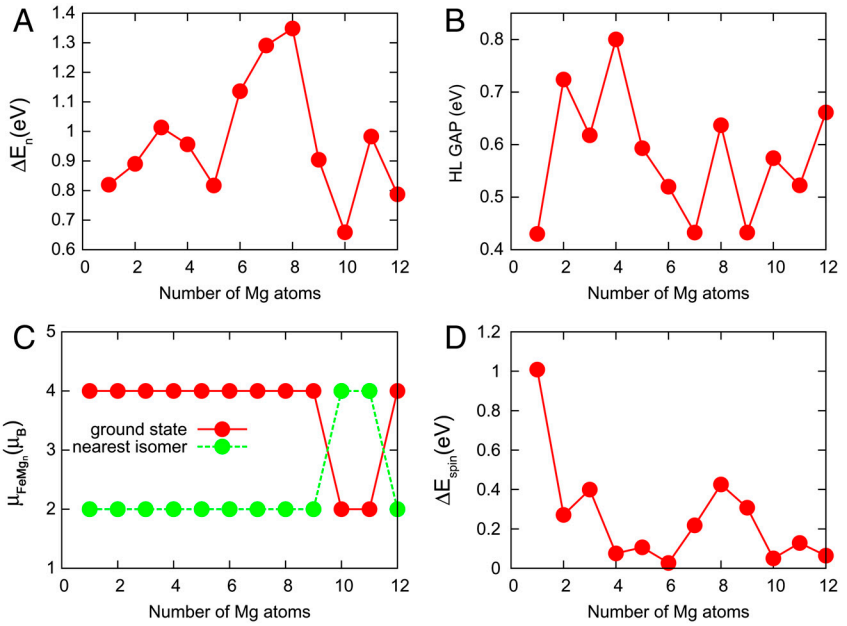


**Fig. 2.** Energetic and magnetic trends of $FeMg_n$. (*A*) Variation of the gain in energy upon successive to addition of Mg atoms ($\Delta E$) with $n$. (*B*) Variation of the HOMO-LUMO gap (HL GAP) with $n$. (*C*) Variation of the magnetic moments ($\mu$) with $n$ for the ground state and nearest isomer with $n$. (*D*) Variation of the relative energy between the ground state and the nearest isomer $\Delta E_{spin}$ as a function of $n$.

calculated the energy $\Delta E_{spin}$ between the ground state and the next isomer of different spin state. Fig. 2*D* shows the variation of $\Delta E_{spin}$ and $FeMg_8$ has a large spin excitation energy showing that the spin state is fairly robust. The reasons underlying the stability, however, still remained open. Because the Fe atom maintains its spin magnetic moment, one could think that a Fe atom contributes 2 sp electrons to the valence pool. Combined with 16 sp electrons from 8 Mg atoms, one could think of $FeMg_8$ as a stable cluster with a shell filling at 18 electrons. To verify if this supposition was correct, we proceeded to examine the nature of molecular orbitals.

Fig. 3 shows the one electron levels and the electronic orbitals associated with each level for the spin up and down configurations. The pictures show the plots of the electron wave function and can help identify the nature of orbitals. Starting from the lowest state in the majority spin, one notices states of increasing angular momentum. The lowest state is spread out over several atoms and has 1S superorbital character. The first two electrons occupy majority and minority S states. The next two states have 1P character. These are followed by four D orbitals. A Mulliken analysis indicates that these D orbitals have 20% contribution from the Fe site and the remaining from the Mg atoms. The set of D orbitals is followed by a $P_z$ orbital and a D orbital of $Dz^2$ symmetry. These states are followed by the 2S state. The $1S^2$, $1P^6$, $1D^{10}$, and $2S^2$ states of both spins are filled with 20 valence electrons coming from Fe and Mg sites and one is left with 4 of the total of 24 valence electrons. In a homogeneous confined nearly free electron gas (jellium model for a homogeneous cluster), this sequence is followed by a 1F supershell. Here, the presence of Fe site leads to a 2D set of orbitals. Because there are five degenerate D orbitals in a spherical atom, the stability of the species with four majority electrons is intriguing. The answer lies in the shape of the cluster. The Mg cores in $FeMg_8$ have a square antiprism arrangement as seen in Fig. 1. As we recently showed, the degeneracy in the P, D… electronic states can be broken by the potential of the ionic cores forming the cluster and can lead to highly stable species at subshell filling (27).

In the present case, the D states are split into a group of 4 ($D_{xy}$, $D_{x^2-y^2}$, $D_{xz}$, and $D_{yz}$) and a $D_{z^2}$ state leading to a stable species with four unpaired electrons shown in a red dotted square in Fig. 3. To provide further support for the crystal field effects, we distorted the Mg sites to form a regular cubic structure. The pairing of the D orbitals changed into groups of 3 and 2. This is like the splitting of atomic d states into $t_{2g}$ and $e_g$ states in a cubic field in solids. Unlike the crystal field effects in solids, here, the field is generated by the ionic cores and hence is internal to the system. The ability of clusters to acquire stability through suborbital splittings via the internal ionic rearrangements is quite unique and, in this case, results in magnetic species with a spin magnetic moment of 4.0 $\mu_B$. The 2D states have a node in the center and are again composed of atomic d states of the Fe atom mixed with D states of the confined nearly free electron gas. A Mulliken population analysis again indicates that the 2D states have almost 85% contribution from the Fe d states. To further demonstrate Hund's rule filling of D shells in cluster superatoms, we carried out a study of the spin magnetic moment of $TMMg_8$ where all the 3d-TM atoms were tested. The results are shown in Fig. 4*A*. $ScMg_8$ has a configuration $1S^2\ 1P^6\ 1D^{10}\ 2S^1$, and $TiMg_8$ is the first cluster in the series with a 20-electron closed-shell configuration $1S^2\ 1P^6\ 1D^{10}\ 2S^2$. Further addition of d electrons results in filling of the 2D subshell to a configuration of $2S^1\ 2D^4$ in the Mn atom.

The transition metal d states hybridize with the superatomic-orbital D states resulting in the splitting between the majority and minority sets of the nearly free electron gas supershells. Fig. 4*B* shows the energy difference between the lowest majority and minority states of the 1S, 1D, 2S, and 2D supershells (exchange splitting) in the $TMMg_8$ (TM = Sc, Ti, V, Cr, Mn, Fe, Co, and Ni) clusters, and the corresponding exchange splitting in the 3d TM atoms. It can be seen that the splitting in the TM atoms is the driving force for the splitting of the supershells. This demonstrates Hund's rule in the $TMMg_8$ clusters and further

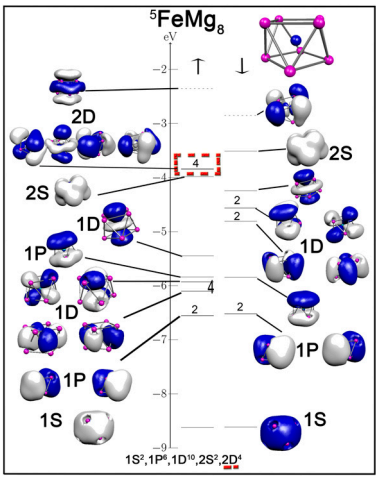


**Fig. 3.** One electron energy levels and orbital wavefunction isosurfaces (isoval = 0.01 a.u.) in the $FeMg_8$ cluster. The majority and minority levels are shown. Continuous lines correspond to the filled levels, whereas the dotted lines correspond to the unfilled states. For each level, the angular momentum of the supershells has been marked. The 2D occupied supershell is highlighted in a red dotted square. The ground-state geometry of the $FeMg_8$ cluster is also shown.

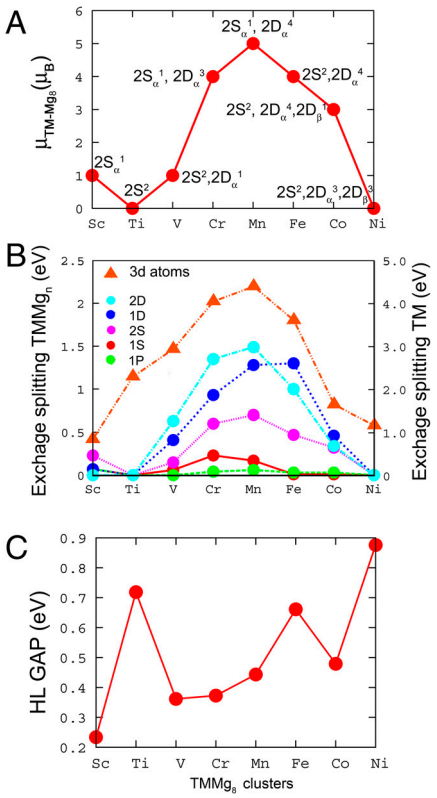


**Fig. 4.** Energetic and magnetic trends of $TMMg_8$ (TM = Sc, Ti, V, Cr, Mn, Fe, Co, and Ni) clusters and of TM 3d ground states. (*A*) Variation of the magnetic moments (μ) of $TMMg_8$ with TM. The angular character of the two topmost levels and their occupancy are also given. (*B*) Variation of the exchange splitting of the 1S, 1P, 1D, 2S and 2D supershells of $TMMg_8$ with TM (circles), and for the TM 3d atoms ground states (orange triangles). (*C*) Variation of the HOMO-LUMO gap (HL GAP) of $TMMg_8$ with TM.

shows how the splitting can be controlled by the nature of the central atom.

Because the splitting between S orbitals is small as seen in Fig. 4*B*, the $Mg_8Mn$, although having a large spin magnetic moment of 5 $\mu_B$, does not have a large HOMO-LUMO gap. Going to Fe overcomes this deficiency leading a stable species with a closed-shell free electron configuration of 20 electrons ($1S^2$ $1P^6$ $1D^{10}$ $2S^2$) and four alpha 2D electrons ($2D^4$). $FeMg_8$ then presents a maximum in the HOMO-LUMO gap of 0.64 eV in the $TMMg_8$ series as shown in Fig. 4*C*. Figs. S1 and S2 reinforce our findings showing the one electron energy levels and molecular orbital wavefunctions for the $TMMg_8$ series, along with the superatom shell configuration for each $TMMg_8$ species.

Because the Mg atoms are marked by s- and p-valence atomic orbitals while the transition metal atoms have s, p-, and d-atomic orbitals, one may question if the above findings could be rationalized within a localized orbital framework. The tensor surface harmonic (TSH) theory introduced by Stone (28) and later developed by Mingos, Wales, and others (29–31) does provide such a framework that can also be used to study structural rearrangements (32). Here, we reconsider the case of $FeMg_8$. We focus on the electronic shells formed from the *s* and *p* orbitals of the Mg atoms. Note that the atomic 3d orbitals centered at the Fe site can be regarded as bystander. The s orbitals centered at the Mg site form 1S, 1P, and 1D orbitals, whereas the radial $p_z$ orbitals could be considered as contributing to the 2S orbital. The 2D orbitals hybridize with the 3d orbitals to undergo an exchange splitting that results in the stabilization of the four unpaired electrons. It will be interesting to examine if the TSH framework could be applied to understand the stability and electronic character of other superatoms.

The formation of stable magnetic species does raise the question if such clusters would maintain the magnetic characteristics when assembled to form molecules or bigger clusters, and how do the magnetic moments couple in such aggregates? There are several approaches to make cluster assemblies from superatoms. One could isolate clusters by passivating them with organic ligands (14, 15), insert them into zeolite cages (33), or deposit them on substrates (34). Forming assemblies through direct deposition on substrates, however, requires the magnetic features to be maintained through the assembly. Consequently, we examined the evolution of geometry and the magnetic properties as two $Mg_8Fe$ clusters were brought together starting at large separation. Fig. S3 shows the lowest energy structure of the composite cluster and the next higher magnetic state. The lowest energy structure of the cluster molecule is an antiferromagnetic species where the individual clusters maintain the geometrical arrangement of free clusters. The state is followed by a quintuplet configuration that is 0.18 eV higher in energy. The localized moments on the Fe atoms in the quintuplet have unequal magnitudes. The resulting structures indicate that the superatoms are likely to maintain their identity upon assembly.

The present work offers a strategy to design magnetic motifs in the superatom family via inducing exchange splitting through hybridization of the atomic d states of the Fe atom with the superatomic D states. The hybridization leads to a large exchange splitting of the D-superatom orbitals. The system can be further stabilized by using the electrostatic field of the Mg ions as the crystal field split the D state into a group of 4 and 1 leading to stable $Mg_8Fe$ species with a large HOMO-LUMO gap. Attempts to make a $(Mg_8Fe)_2$ supermolecule indicate that the individual clusters do retain their shapes and the molecule is marked by a small energy difference between the ferromagnetic and antiferromagnetic states. Our previous work shows that such units have the potential for spin polarized currents through application of small fields (35). Although the full potential of such applications will form the basis of future work, a preliminary density of states was obtained by broadening the molecular levels by Gaussians of width 0.2 eV (see Fig. S4). The majority spin density of states at the Fermi energy is much higher than the minority states in the ferromagnetic state! As the current passes through Mg sites, the lack of spin orbit coupling is likely to enhance spin coherence over longer distances. We hope that the present work combining magnetism and semiconducting features arising from combination of motifs with filled shells will serve as the starting point for further systematic search for such species.

## Methods

The theoretical studies were carried out using a linear combination of atomic orbitals molecular orbital approach within a gradient corrected density functional approach (36–39). The molecular orbitals are expressed as a linear combination of Gaussian functions centered at the atomic sites. For each cluster size, the ground-state configuration was obtained by starting from several initial configurations and moving the atoms in the direction of forces to minimize the energy. A frequency analysis was carried out to ascertain the stability of the ground state, and various spin configurations were attempted to find the ground state. Details of the theoretical procedures are provided in *SI Text*.

**ACKNOWLEDGMENTS.** We are grateful to Dr. Mark R. Pederson for all the discussions and for valuable suggestions. We gratefully acknowledge support from US Department of Energy.

1. Knight WD, Clemenger K, de Heer Saunders WA, Chou MY, Cohen ML (1984) Electronic shell structure and abundances of sodium clusters. *Phys Rev Lett* 52:2141–2143.
2. Martins JL, Car R, Buttet J (1981) Variational spherical model of small metallic particles. *Surf Sci* 106:265–271.
3. Hintermann A, Manninen M (1983) Feasibility of cluster calculations in describing impurities in simple metals. *Phys Rev B Condens Matter* 27:7262–7270.
4. Ekardt W (1984) Work function of small metal particles—Self-consistent spherical jellium-background model. *Phys Rev B Condens Matter* 29:1558–1564.
5. Leuchtner RE, Harms AC, Castleman AW, Jr. (1989) Thermal metal cluster anion reactions—Behavior of aluminum clusters with oxygen. *J Chem Phys* 91:2753–2754.
6. Brack M (1993) The physics of simple metal clusters, self-consistent jellium model and semiclasical approaches. *Rev Mod Phys* 65:677–732.
7. de Heer WA (1993) The physics of simple metal clusters: experimental aspects and simple models. *Rev Mod Phys* 65:611–676.
8. Khanna SN, Jena P (1995) Atomic clusters—Building-blocks for a class of solids. *Phys Rev B Condens Matter* 51:13705–13716.
9. Ashman C, Khanna SN, Kortus J, Kortus J, Pederson MR (2000) *Cluster and Nanostructure Interfaces*, eds P Jena, SN Khanna, and BK Rao (World Scientific, London), pp 383–392.
10. Bergeron DE, Castleman AW, Jr, Morisato T, Khanna SN (2004) Formation of $Al_{13}I^-$: Evidence for the superhalogen character of $Al_{13}$. *Science* 304:84–87.
11. Bergeron DE, Roach PJ, Castleman AW, Jr, Jones NO, Khanna SN (2005) Al cluster superatoms as halogens in polyhalides and as alkaline earths in iodide salts. *Science* 307:231–235.
12. Reveles JU, Khanna SN, Roach PJ, Castleman AW, Jr (2006) Multiple valence superatoms. *Proc Natl Acad Sci USA* 103:18405–18410.
13. Jones NO, et al. (2006) Structural, electronic, and chemical properties of multiply iodized aluminum clusters. *J Chem Phys* 124:154311.
14. Hartig J, Stösser A, Hauser P, Schnöckel HA (2007) Metalloid $[Ga_{23}\{N(SiMe_3)_2\}_{11}]$ cluster: The jellium model put to test. *Angew Chemie Int Ed Engl* 46:1658–1662.
15. Jadzinsky PD, Calero G, Ackerson CJ, Bushnell DA, Kornberg RD (2007) Structure of a thiol monolayer-protected gold nanoparticle at 1.1 Å resolution. *Science* 318:430–433.
16. Castleman AW, Jr, et al. (2007) From designer clusters to synthetic crystalline nanoassemblies. *Nano Lett* 7:2734–2741.
17. Walter M, et al. (2008) Unified view of ligand-protected gold clusters as superatom complexes. *Proc Natl Acad Sci USA* 105:9157–9162.
18. Castleman AW, Jr, Khanna SN (2009) Clusters, superatoms and building blocks of new materials. *J Phys Chem C* 113:2664–2675.
19. Reveles JU, et al. (2009) Designer magnetic superatoms. *Nat Chem* 1:310–315.
20. Pradhan K, Reveles JU, Sen P, Khanna SN (2010) Enhanced magnetic moments of alkali metal coated Sc clusters: New magnetic superatoms. *J Chem Phys* 132:124302.
21. Peppernick SJ, Gunaratne KDD, Castleman AW, Jr (2010) Superatom spectroscopy and the electronic state correlation between elements and isoelectronic molecular counterparts. *Proc Natl Acad Sci USA* 107:975–980.
22. Geguzin II (1981) Spin polarization of high-symmetry clusters of simple metals in the ground state. *JETP Lett* 33:568–570.
23. Reimann SM, Manninen M (2002) *Rev Mod Phys* 74:1283–1342.
24. Khanna SN, Rao BK, Jena P, Martins JL (1987) Jahn-Teller distortion, Hund's coupling and metastability in alkali tetramers. *Physics and Chemistry of Small Clusters*, eds P Jena, BK Rao, and SN Khanna (Plenum Press, New York), pp 435–438.
25. Jellinek J, Acioli PH (2002) Magnesium clusters: Structural and electronic properties and the size-induced nonmetal-to-metal transition. *J Phys Chem A* 106:10919–10925.

26. Pradhan K, Sen P, Reveles JU, Khanna SN (2008) First-principles study of $TMNa_n$ (TM = Cr, Mn, Fe, Co, Ni; $n = 4–7$). *J Phys Condens Matter* 20:255243.
27. Roach PJ, Woodward WH, Reber AC, Khanna SN, Castleman AW, Jr (2010) Crystal field effects on the reactivity of aluminum-copper cluster anions. *Phys Rev B Condens Matter* 81:195404.
28. Stone AJ, Alderton MJ (1982) A new model of structure and bonding in boron hydrides. *Inorg Chem* 21:2297–2302.
29. Mingos DMP (1986) Bonding in molecular clusters and their relationship to bulk metals. *Chem Soc Rev* 15:31–61.
30. Johnston RL, Mingos MP (1987) A group theoretical paradigm for describing the Skeletal Molecular orbitals of cluster compounds. *J Chem Soc Dalton Trans* 3:647–657.
31. Wales DJ, Mingos DMP, Slee T, Lin ZY (1990) Clusters in inorganic and molecular-beam chemistry—Some unifying principles. *Acc Chem Res* 23:17–22.
32. Wales DJ, Stone AJ (1987) Theoretical study of rearrangements in boranes. *Inorg Chem* 26:3845–3850.
33. Mikhailov MN, Kustov LM, Kazansky VB (2008) The state and reactivity of $Pt_6$ particles in ZSM-5 zeolite. *Catal Letters* 120:8–13.
34. Perez A, et al. (1997) Cluster assembled materials: A novel class of nanostructured solids with original structures and properties. *J Phys D Appl Phys* 30:709–721.
35. Haiying H, Pandey R, Reveles JU, Khanna SN, Karna SP (2009) Highly efficient ($Cs_8V$) superatom-based spin-polarizer. *Appl Phys Lett* 95:192104.
36. Koster AM, et al. (2006) deMon2k, V. 2.3.6. (The deMon Developers Community, Cinvestav, Mexico), available at www.deMon-software.com.
37. Pederson MR, Jackson KA (1990) Variational mesh for quantum-mechanical simulations. *Phys Rev B Condens Matter* 41:7453–7461.
38. Jackson K, Pederson MR (1990) Accurate forces in a local-orbital approach to the local-density approximation. *Phys Rev B Condens Matter* 42:3276–3281.
39. Porezag D, Pederson MR (1999) Optimization of Gaussian basis sets for density-functional calculations. *Phys Rev A* 60:2840–2847.

# Supporting Information

## Medel et al. 10.1073/pnas.1100129108

### SI Materials and Methods

**Theoretical Method.** First-principles electronic structure investigations were carried out using a molecular orbital approach within a gradient corrected density functional framework. The molecular orbitals are expressed as linear combinations of atomic orbitals formed via a combination of Gaussian functions centered at the atomic sites. The exchange-correlation contributions are included within a gradient corrected (GGA) density functional as proposed by Perdew et al. (1). The actual calculations were carried out using the deMon2k software (2). For all the atoms we employed the gradient corrected optimized double zeta valence polarized basis set (3) and the GEN-A2 auxiliary function set. The exchange-correlation potential was calculated via a numerical integration on an adaptive grid from the orbital density (4). To determine the geometry and spin multiplicity of the ground state, the configuration space was sampled by starting from several initial configurations and spin multiplicities and optimizing the geometry employing the quasi-Newton Levenberg–Marquardt method (5). All structures were fully optimized in delocalized redundant coordinates without imposing any symmetry constraints, to allow for full variational freedom. The molecular geometries and orbitals were plotted using the Molekel software (6). To eliminate any uncertainty due to the choice of the basis set and the numerical procedure one additional complimentary scheme was used. All electron calculations were carried out, using the Naval Research Laboratory Molecular Orbital Library (NRLMOL) developed by Pederson and coworkers (7–9). Here the Hamiltonian matrix elements are evaluated by numerical integration over a mesh of points. The basis sets, built from a variable number of primitive Gaussians, are based on a total-energy minimization for free atoms and are optimized for all electron density functional calculations (9). The basis sets were supplemented with a diffuse d Gaussian to allow further variational freedom. For details of the codes and the basis sets, the reader is referred to earlier papers (7–9). In general we found a very good agreement between the deMon2k and NRLMOL calculations. The results presented in the paper are based on the deMon2k calculations, with the exception of the $(FeMg_8)_2$ dimer for which the ferromagnetic and antiferromagnetic states were calculated with the NRLMOL code.


1. Perdew JP, Burke K, Enzerhof M (1996) Generalized gradient approximation made simple. *Phys Rev Lett* 77:3865–3868.
2. Koster AM, et al., (2006) deMon2k, V. 2.3.6 (The deMon Developers Community, Cinvestav, Mexico), available at www.deMon-software.com.
3. Calaminici P, Janetzko F, Köster AM, Mejia-Olvera R, Zuniga-Gutierrez B (2007) Density functional theory optimized basis sets for gradient corrected functionals: 3d transition metal systems. *J Chem Phys* 126:044108.
4. Köster AM, Flores-Moreno R, Reveles JU (2004) Efficient and reliable numerical integration of exchange-correlation energies and potentials. *J Chem Phys* 121:681–690.
5. Reveles JU, Köster AM (2005) Geometry optimization in density functional methods. *J Comput Chem* 25:1109–1116.
6. Flükiger P, Lüthi HP, Portmann S, Weber J. (2000) *Molekel 4.0* (Swiss National Supercomputing Centre CSCS, Manno, Switzerland).
7. Pederson MR, Jackson KA (1990) Variational mesh for quantum-mechanical simulations. *Phys Rev B Condens Matter* 41:7453–7461.
8. Jackson K, Pederson MR (1990) Accurate forces in a local-orbital approach to the local-density approximation. *Phys Rev B Condens Matter* 42:3276–3281.
9. Porezag D, Pederson MR (1999) Optimization of Gaussian basis sets for density-functional calculations. *Phys Rev A* 60:2840–2847.

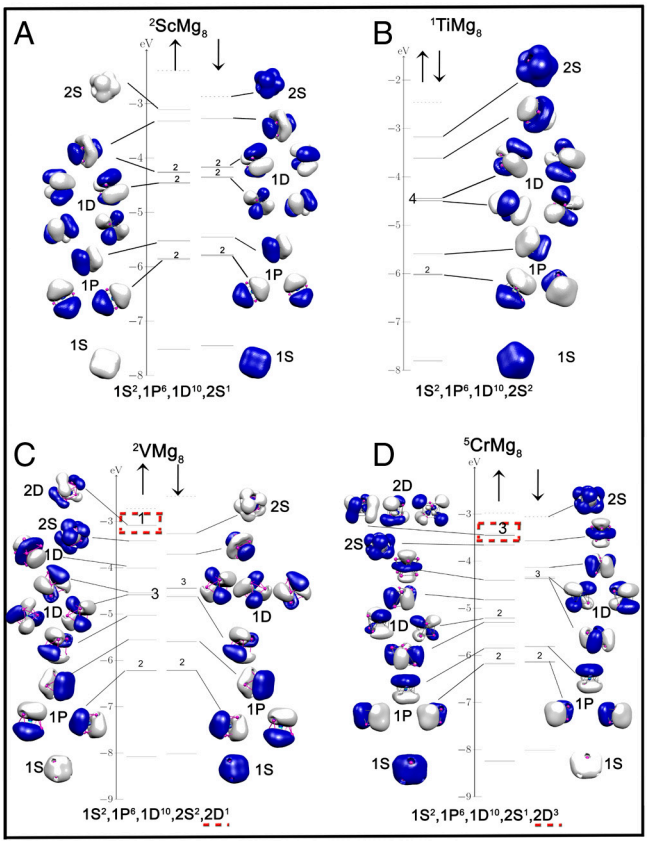


**Fig. S1.** The one electron energy levels and orbital wavefunction isosurfaces (isoval = 0.01 a.u.) in the $TMMg_8$ clusters. (*A*) TM = Sc, (*B*) TM = Ti, (*C*) TM = V, and (*D*) TM = Cr. The majority and minority levels are shown. Continuous lines correspond to the filled levels, whereas the dotted lines correspond to the unfilled states. For each level, the angular momentum and their occupancy has been marked. The 2D occupied energy levels are highlighted in a dotted red box.

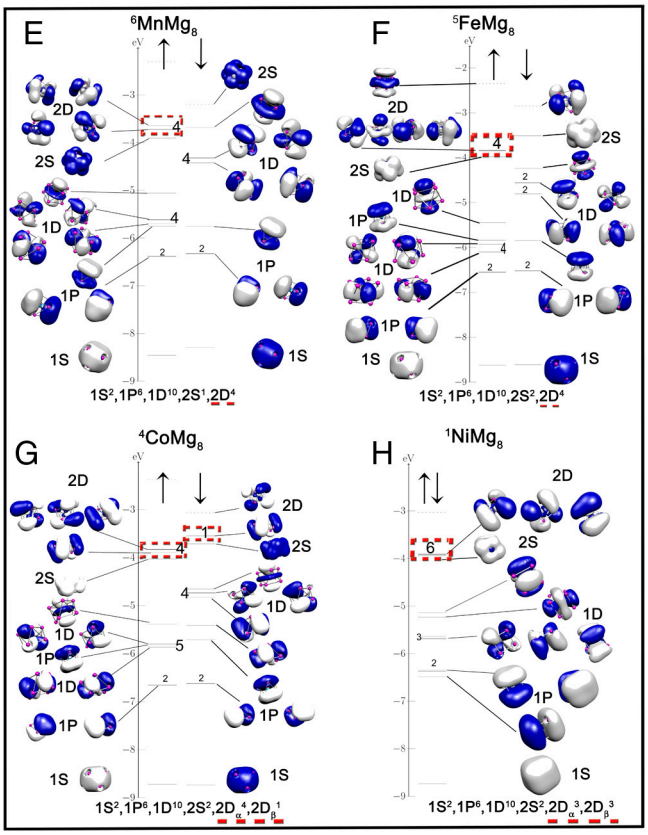


**Fig. S2.** The one electron energy levels and orbital charge wavefunction isosurfaces (isoval = 0.01 a.u.) in the $TMMg_8$ clusters. (*E*) TM = Mn, (*F*) TM = Fe, (*G*) TM = Co, and (*H*) TM = Ni. See caption of Fig. S1.

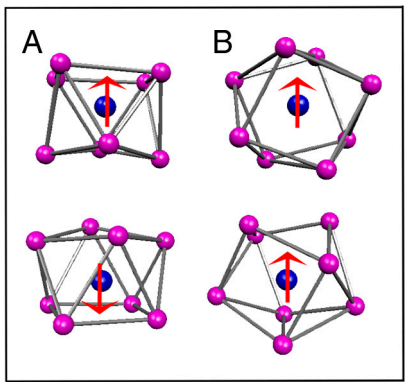


**Fig. S3.** The lowest energy structure and next spin isomer of the $(FeMg_8)_2$ dimer. (*A*) The antiferromagnetic (0 $\mu_B$) and (*B*) the ferromagnetic state (4 $\mu_B$) state. Arrows indicate the direction of Fe local spin moments.

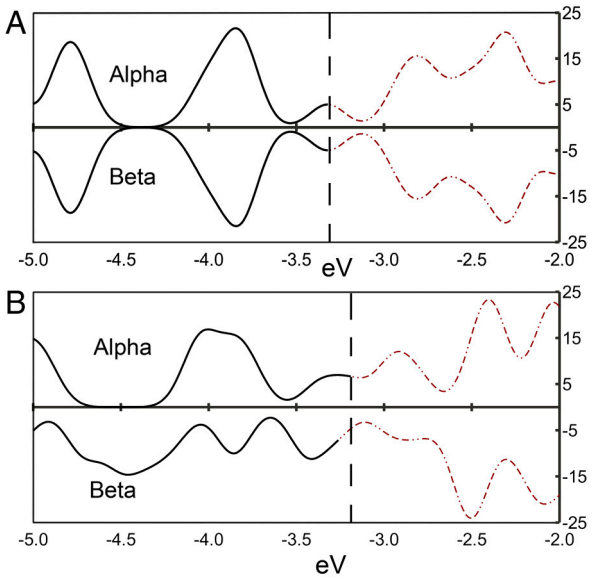


**Fig. S4.** The density of states for the lowest energy structure and next spin isomer of the $(FeMg_8)_2$ dimer. (*A*) The antiferromagnetic (0 $\mu_B$) and (*B*) the ferromagnetic (4 $\mu_B$) state. The Fermi level is marked with a dotted line.